Int. J. Electrochem. Sci., 16 **(2021)** Article Number: 211139, doi: 10.20964/2021.11.15

International Journal of
ELECTROCHEMICAL
SCIENCE
www.electrochemsci.org

Corrosion Inhibition of N80 Steel by Newly Synthesized Imidazoline Based Ionic Liquid in 15% HCl Medium: Experimental and Theoretical Investigations

Lei Guo[1,2], *Mengyue Zhu*[3], *Jun Chang*[2,*], *Renjith Thomas*[4], *Renhui Zhang*[3], *Pengjie Wang*[3], *Xingwen Zheng*[5], *Yuanhua Lin*[1,*] *Riadh Marzouki*[6,7]

[1] State Key Laboratory of Oil and Gas Reservoir Geology and Exploitation, Southwest Petroleum University, Chengdu 610500, Sichuan, China
[2] School of Material and Chemical Engineering, Tongren University, Tongren 554300, China
[3] School of Materials Science and Engineering, East China Jiaotong University, Nanchang 330013, China
[4] Department of Chemistry, St Berchmans College (Autonomous), Changanassery 686101, Kerala, India
[5] Key Laboratory of Material Corrosion and Protection of Sichuan Province, Zigong 643000, China
[6] Chemistry Department, College of Science, King Khalid University, Abha 61413, Saudi Arabia
[7] Chemistry Department, Faculty of Sciences, University of Sfax, 1171 Sfax 3000, Tunisia
[*]E-mail: junchang85@163.com, yhlin28@163.com

Received: 1 August 2021 / *Accepted:* 4 September 2021 / *Published:* 10 October 2021

An imidazoline based ionic liquid, namely 2-heptadecyl-3-butyl-3-((n-methyl-thiourea) ethyl)-1H-imidazole-3-ammonium (MTOI), was prepared by a simple synthesis route. The structure of MTOI was characterized by FTIR testing. Electrochemical techniques and surface analysis tests were used to explore the corrosion inhibition behavior of MTOI on N80 steel in 15% HCl solution. The results showed that the adsorption of MTOI on the surface of N80 steel was in accordance with Langmuir isotherm, and it belongs to the mixed-type inhibitor with the maximum inhibition efficiency of 97% at 90 ppm. SEM-EDS measurement verified that the N and S atoms in the ionic liquid were exactly adsorbed on the metal surface. Besides, the active nature of MTOI molecule was revealed by density functional theory (DFT) calculations, and the adsorption behavior of MTOI molecule on surface of N80 steel was elucidated by molecular dynamics (MD) simulations. This work can provide beneficial guidance for the future research of efficient and environmentally friendly ionic liquid corrosion inhibitors.

Keywords: Ionic liquid, Corrosion inhibition, N80 steel, Electrochemical techniques, Molecular simulation

1. INTRODUCTION

N80 steel has the advantages of excellent strength and toughness. N80 casing is an important equipment in the oil drilling process. However, the application process of oil well pipe will produce calcium salts, which can clog the pipe hole and cause serious oil pipe leakage. The oil pipeline leak has caused great damage to the environment and economy. HCl solution (15~28%) is commonly used to dissolve sediments in oil well pipes to facilitate the flow of crude oil and increase recovery from depleted wells [1]. Unfortunately, high concentration hydrochloric acid solution is easy to form ferric chloride compound with tubing steel, resulting in serious corrosion of tubing. Hence, the corrosion is usually delayed by adding suitable inhibitor to HCl medium. Inorganic corrosion inhibitors such as phosphate, borate and tungstate are widely developed and used in the market [2]. But its dosage is large, and the heavy metal content may cause serious environmental pollution. Therefore, the low-toxicity organic corrosion inhibitor has aroused much attention recently [3-5].

Ionic liquid is a molten salt composed of organic cations and small anions. It has excellent water solubility, thermal & chemical stability, and thus can be a candidate for green corrosion inhibitors. The inhibition performance depends heavily on the electron-donating capacity of heteroatoms (N, O, S, P) in the polar functional segments as well as the length of hydrophobic alkyl chain [6, 7]. Farag et al. researched the corrosion suppression of thiazole ionic liquid on carbon steel in hydrochloric acid solution [8]. The electrochemical results showed that the maximum inhibitory effect of 40 ppm inhibitor was 91.4%. Kannan et al. investigated the corrosion inhibition performance and mechanism of ionic liquid benzyltributylammonium tetrachloroaluminate on carbon steel in 2 M HCl medium [9]. At the optimal concentration of 400 ppm, the inhibitor displayed excellent inhibition performance (97%). Their theoretical calculations show that the cation of the ionic liquid is adsorbed on the metal surface through the bridge of the anion, which can prevent the corrosion. Schmitzhaus and co-workers evaluated the corrosion performance of *N*-methyl-2-hydroxyethylam monium oleate for mild steel in 0.1 M HCl medium [10]. The surface analysis confirmed that the self-assembled inhibitor film modified the wettability of steel surface, exhibiting a more hydrophobic behavior. Owing to the background above, it is still necessary to develop alternative economical and environmentally friendly ionic liquid based corrosion inhibitors, and especially the inhibition mechanism deserves further exploration.

Therefore, in this work, we synthesized a novel imidazoline based ionic liquid (MTOI for short). Fourier transform infrared spectrophotometry (FTIR) technique was employed to characterize the structure of MTOI. Electrochemical impedance spectroscopy (EIS) and potentiodynamic polarization curves (PDP) were performed to examine the corrosion inhibition performance for N80 steel in 15% HCl solution. The morphology of the steel surface was studied by SEM-EDS measurement. In addition, the experimental results were further verified by theoretical calculations in order to understand the inhibition mechanism.

2. EXPERIMENTAL

2.1. Materials and chemicals

All analytical pure reagents, such as oleic acid, diethylenetriamine, *n*-iodobutane, methyl thiourea, and concentrated HCl (36~38%), were purchased from Aladin Reagents Co., Ltd. The N80 steel chemical composition is the following: C (0.45%), Mn (1.70%), Si (0.32%), P (0.014%), S (0.013%), Cu (0.12%), Ni (0.04%), Cr (0.03%), Mo (0.20%), and the rest of the Fe. The N80 steel used for the test was a cylinder of Φ16×5 mm. Before the test, it was polished by sandpaper with different grades (120~1000), followed by ultrasonic cleaning with deionized water, ultrasonic removal of grease with anhydrous ethanol, and cold air drying. During the test, the area of N80 steel burst in the corrosive medium was 1 cm^2. Deionized water was made in laboratory.

2.2. Preparation and characterization of MTOI compound

The ratio of oleic acid to diethylenetriamine was 1:1.1 as the reactant, and added into the three-nosed flask. First, it was heated at 140 ℃ for 2 h to amide, then heated to 210 ℃ for 1.5 h. The water separated by xylene was used to complete the closed-loop reaction to form imidazoline oleate. The synthesis of imidazoline oleate was reacted with *n*-iodobutane and methyl thiourea at 140 ℃ for 1.5 h. At the end of the reaction, the product mixture was cooled down to room temperature. The purified product MTOI is obtained by vacuum distillation to remove the unreacted reactants and the generated water. The whole reaction process is shown in Scheme 1. Fourier transform infrared spectroscopy (IRaffini-1S, Japan) was used to characterize the structure of MTOI. The resolution and wave number range of FTIR spectrum acquisition are 1 cm^{-1} and 4000~500 cm^{-1}, respectively.

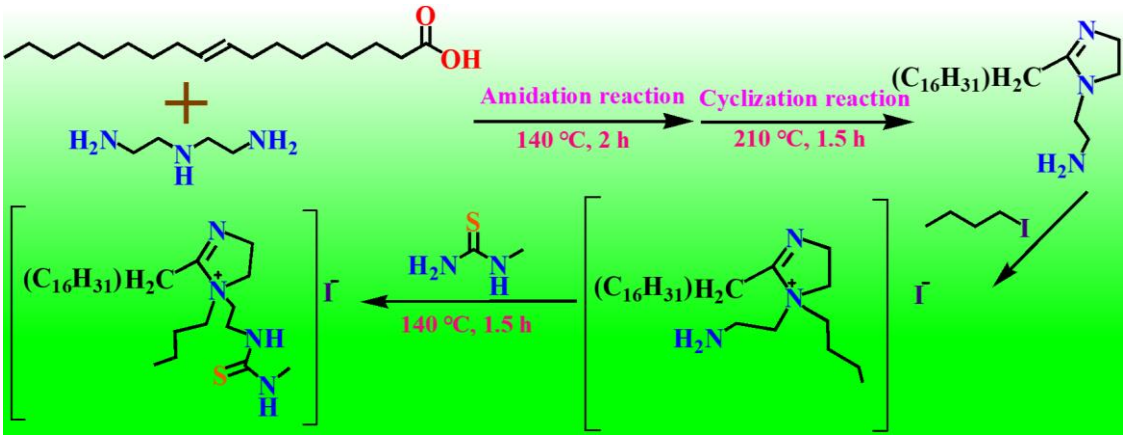

Scheme 1. Synthesis route of oleic acid imidazoline derivatives (MTOI).

2.3. Electrochemical experiments

Electrochemical experiments were evaluated by CHI660E workstation from Shanghai Chenhua Instruments Co., Ltd. A standard three-electrode system was applied in the all experiment. N80 cylinder

steel was regarded as the working electrode, the inert platinum deem as the counter electrode, and the reference electrode choose the saturated calomel electrode (SCE). The open circuit potential was tested for 0.5 h without current input before the electrochemical test, so that the system could reach a stationary state within the fluctuation range of 10 mV. Electrochemical impedance spectroscopy was obtained from a previously stable open circuit potential and measured in the frequency range of 100 kHz~10 mHz. The range of potentiodynamic polarization was measured from −250 mV to +250 mV at the open circuit potential (E_{ocp}), and the scanning rate was 0.167 mV s^{-1}. The electrochemical data were fitted by ZsimpWin 3.6 software. The whole process of electrochemical tests was evenly triplicate to reduce experimental error at room temperature 298 K.

2.4. Surface analysis

The N80 steel is pretreated by grinding and polishing with different grades of sandpaper (120 ~5000), washing by water, ultrasonic cleaning with anhydrous ethanol, and cold air drying. The steel was immersed in 15% HCl without or with MTOI for 6 h, and the pretreatment and repeated cleaning steps were carried out. SEM (JEO-JSM-7800F, Japan) was applied to analyze component and surface morphology of N80 steel under different conditions.

2.5. Theoretical details

2.5.1. DFT calculations

The molecule was subjected to geometry optimization using density function theory with the B3LYP/aug-cc-pVDZ basis set using Gaussian software. Frequency calculations were performed and no imaginary frequency has been observed indicating that the optimized geometry obtained corresponds to a minima. The effect of the water solvent is studied by using IEFPCM model with implicit water solvation atmosphere [11]. The quantum chemical descriptors of MTOI were elicited and analyzed, including E_{HOMO}, E_{LUMO}, ΔE (gap energy), global hardness (ξ), ionisation potential (I), electron affinity (A), ω (electronegativity), and fraction of electrons (ΔN).

2.5.2. Molecular dynamics (MD) simulation

The adsorption behavior of MTOI on iron surface was studied by Forcite module with Materials Studio package [12]. The studied system consisted of Fe(110) surface, one MTOI molecule, and 600 H_2O molecules. Amorphous Cell module was used to construct simulation system, and the size of the simulation box of the system was 24.8 × 24.8 × 39.1 $Å^3$ with periodic boundary condition. The COMPASS was selected as the simulation force field [13], and the simulation was carried out at 298 K under the regular ensemble (NVT), with a time step of 1.0 fs and a total simulation time of 500 ps. All the iron atoms of the substrate were fixed during the calculation process, keeping the adsorbed molecules

interacting freely with the metal surface. More details about MD simulation procedure can be found elsewhere [14-16].

3. RESULTS AND DISCUSSION

3.1. FTIR of MTOI inhibitor

The FTIR spectrum of MTOI inhibitor is shown in Figure 1. The absorption characteristic peak of MTOI is observed to be N−H stretching vibration peak at 3293.0 cm^{-1}, $-CH_2-$ and $-CH_3$ stretching vibration peak at 2923 cm^{-1} and 2852 cm^{-1}, C=N and N−C=S stretching vibration characteristic peak at 1602 cm^{-1} and 1456 cm^{-1}, respectively [17, 18]. Therefore, the FTIR results declare that MTOI inhibitor is successfully synthesized.

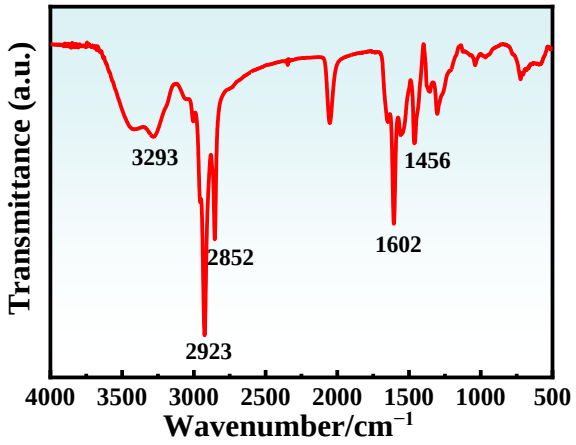

Figure 1. FTIR of the MTOI inhibitor.

3.2. Potentiodynamic polarization analysis

Tafel polarization curve is widely used in electrochemistry, especially in the study of corrosion. Figure 2 depicts the open-circuit potential (OCP) and Tafel curves of the N80 steel without and with different concentrations of MTOI in 15% HCl medium at 298 K. As shown in Figure 2a, with the extension of immersion time, the OCP of the N80 steel in the blank condition presents a positive deviation at first, and then gradually stabilized. However, when 30 ppm of MTOI inhibitor was added, the OCP value shows a negative shift and then became stable. At the same time, with the increase of the concentration of MTOI, the OCP displays a relatively negative deviation compared with the blank solution. These phenomena indicate that the corrosion reaction is affected by the adsorption of inhibitor molecule on the surface of N80 steel. Figure 2b presents the polarization plots with different concentrations of MTOI on N80 steel in 15% HCl. The parameters of corrosion potential (E_{corr}), corrosion current density (i_{corr}), anode slope (β_a), and cathode slope (β_c) were obtained by the extrapolation of Tafel curves, and summarized in Table 1.

Compared with the blank condition, the corrosion current density of anode and cathode can be inhibited simultaneously by adding different concentrations of MTOI, showing that MTOI can inhibit the anodic dissolution and cathodic oxygen evolution of N80 steel. Moreover, the slopes of anode and cathode didn't produce significant changes, which suggests that the corrosion mechanism is not changed [19]. Generally, there is a fundamental law that if the change of E_{corr} value with the addition of inhibitor more than 85 mV can be defined as anode or cathode inhibitor, otherwise, it is a mixed type corrosion inhibitor [20, 21].

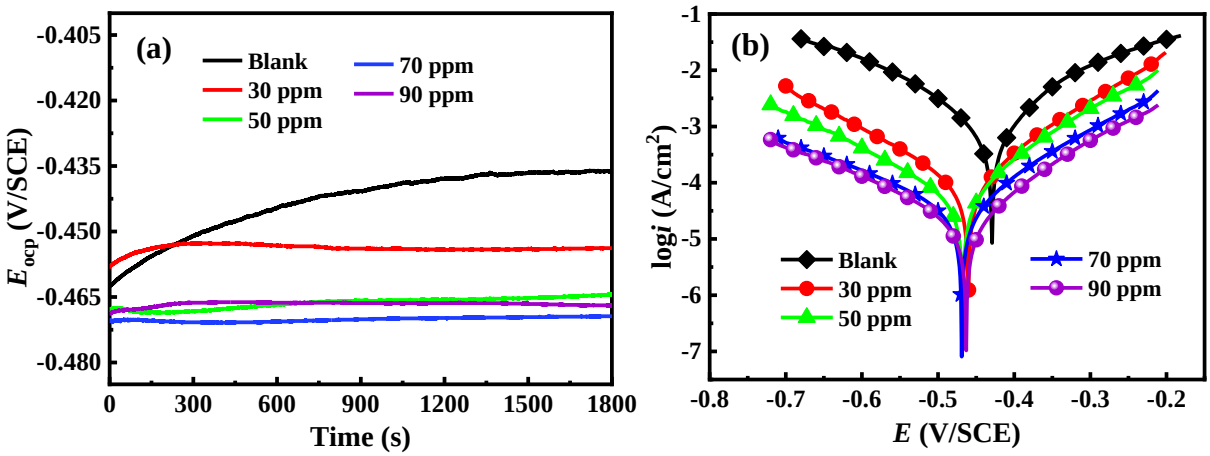

Figure 2. Electrochemical test of N80 steel in 15% HCl without and with different concentrations of MTOI inhibitor: (a) OCP and (b) Tafel curves.

Table 1. Potentiodynamic polarization parameters for N80 steel immersed in 15% HCl solution in the absence and presence of different concentrations of MTOI inhibitor.

C (ppm)	E_{corr} (V SCE^{-1})	i_{corr} (μA cm^{-2})	β_a (mV dec^{-1})	$-\beta_c$ (mV dec^{-1})	η_{PDP} (%)
Blank	−0.433	800.8	118	157	
30	−0.460	90.9	100	137	88.7
50	−0.468	58.3	102	152	92.7
70	−0.469	32.6	108	176	95.9
90	−0.463	18.5	101	149	97.7

According to the values in Table 1, the change of corrosion potential of MTOI with different concentrations is not more than 85 mV, suggesting that MTOI is a mixed inhibitor. Therefore, we can conclude that the blocking effect in the restrain process is stronger than the energy effect, and thus the former plays a dominant role. Table 1 also records the corrosion inhibition efficiency (η_{PDP}), which is calculated by [22]:

$$\eta_{PDP} = \frac{i_{corr,0} - i_{corr}}{i_{corr,0}} \times 100\% \qquad (1)$$

where $i_{corr,0}$ and i_{corr} represent the corrosion current densities of N80 steel without and with inhibitor, respectively. We can see that with the increase of MTOI concentration, the inhibition performance becomes better. When the concentration is 90 ppm, the inhibition efficiency reaches 97.7%.

3.3. Electrochemical impedance spectroscopy (EIS)

The Nyquist and Bode diagrams of N80 steel in 15% HCl without and with MTOI inhibitor are displayed in Figure 3. It is clear from Figure 3a that all the Nyquist plots maintained a similar shape for all concentration and appear as single oblate capacitive loop, which infers that the corrosion of steel is dominantly manipulated by the charge transfer process [23].

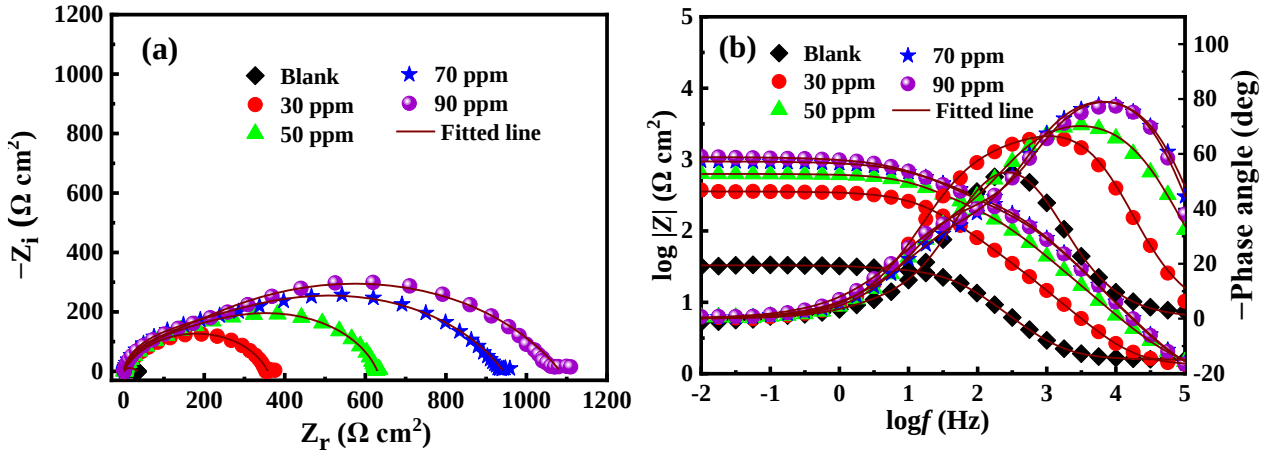

Figure 3. (a) Nyquist and (b) Bode diagrams for N80 steel with different concentrations of MTOI in 15% HCl.

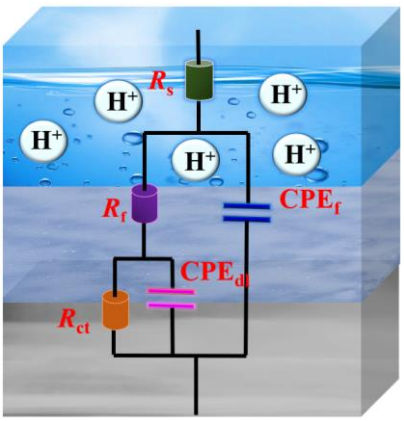

Figure 4. Corresponding equivalent circuit applied to fit the impedance data.

Moreover, the depressed capacitive loop can be ascribed to the frequency dispersion which referred to the heterogeneity and roughness of steel surface [24]. The capacitive loop diameter increases with increasing of the concentration of MTOI compound, which reflects the generation of blocked film

due to the adsorption of MTOI on the metal substrate. As shown in Figure 3b, the Bode phase plots also shows two different peaks, representing the existence of two corresponding time constants in the corrosion process of N80 steel. The phase angle values were found to increase with the MTOI concentration increasing due to the decrease in capacitance rate of the steel surface, making its surface less susceptible to dissolution in corrosive medium.

The equivalent circuit fitted the experimental data is presented in Figure 4, Table 2 listed the EIS descriptors. The equivalent circuit consists of a solution resistance (R_s), a film resistance (R_f), a film constant phase element (CPE_f), an electron transfer resistance (R_{ct}), and a double-layer constant phase element (CPE_{dl}). The polarization resistance (R_p) includes R_f and R_{ct}. The chi-square (χ^2) values are all in the range of 10^{-4}, which confirms that the fitted data and the experimental data are in good agreement. We can see that the R_s values are very small, which confirms that the IR drop could be neglect. CPE replaces the ideal capacitance due to the non-uniformity of the electrode surface, and can be obtained by the following equation [25]:

$$Z_{CPE} = Y_0^{-1}(j\omega)^{-n} \quad (2)$$

where Y_0 represents CPE magnitude, n denotes deviation parameter, j is imaginary root, and ω represents angular frequency. The double layer capacitance (C_{dl}) and inhibition efficiency (η_{EIS}) can be acquired by the following formulas [26, 27]:

$$C_{dl} = (Y_0 R_p^{1-n})^{-n} \quad (3)$$

$$\eta_{EIS} = \frac{R_p - R_{p,0}}{R_p} \times 100\% \quad (4)$$

where $R_{p,0}$ and R_p are polarization resistance in the absence and presence of the inhibitor, respectively.

Table 2. EIS parameters for N80 steel corrosion in the absence and presence of different concentrations of MTOI.

C (ppm)	R_s (Ω cm^2)	CPE_f		C_f (μF cm^{-2})	R_f (Ω cm^2)	CPE_{dl}		C_{dl} (μF cm^{-2})	R_{ct} (Ω cm^2)	χ^2 (10^{-4})	θ	η_{EIS} (%)
		Y_0 (10^{-6} S s^n cm^{-2})	n_1			Y_0 (10^{-6} S s^n cm^{-2})	n_2					
Blank	1.57	256.7	0.86	115.0	28.1	2376	0.81	764.1	3.34	1.51		
30	1.31	31.4	0.87	12.8	79.8	71.8	0.69	12.3	276.9	3.57	0.912	91.2
50	1.10	12.3	0.86	4.9	280.3	66.6	0.78	23.0	348.7	2.17	0.950	95.0
70	0.91	2.6	0.95	1.7	237.8	66.5	0.67	14.7	704.6	3.72	0.967	96.7
90	1.01	2.3	0.97	1.8	178.6	66.6	0.65	14.6	904.7	9.04	0.971	97.1

According to the data in Table 2, compared with the blank, as the concentration increases, the R_{ct} and R_f values increase, leading to increase in inhibition efficiency. A maximum η_{EIS} value was obtained as 97.1%. While the CPE_{dl} and CPE_f values were trending downward, which can be explained by the Helmholtz model [28]:

$$C_{dl} = \frac{\varepsilon_0 \varepsilon}{d} S \quad (5)$$

wherein, ε_0 implies the dielectric constant in the vacuum, ε means permittivity of protective layer, S represents the effective area of immersion, and d is the thickness of the adsorption film. The decrease

of C_{dl} can be ascribed to the increase of d value. These MTOI molecules can be adsorbed on the electrode surface, reducing the contact between the metal and the corrosive medium, and lowering the electrochemical reaction ability of the electrode surface.

3.4. Adsorption isotherm studies

Adsorption isotherms are widely used to predict the nature of interaction of the inhibitors on the metal surface by the mechanism of adsorption. The adsorption behavior of MTOI compound towards the steel substrate can be elucidated by employing diverse isothermal models, in which Langmuir adsorption isotherm provided the most appropriate model fit to the experimental results with linear regression coefficient R^2 (0.9993) near to unity (Figure 5). It can be described as [29]:

$$\frac{C}{\theta} = \frac{1}{K_{ads}} + C \qquad (6)$$

where C denotes the inhibitor concentration, θ refers to the corresponding surface coverage, and K_{ads} represents the adsorption equilibrium constant. The θ value was derived from the η_{EIS} data measured from EIS. Our calculated K_{ads} value for MTOI inhibitor is 1004.22 g/L. In thermodynamic process, Gibbs free energy (ΔG^0_{ads}) can be used to determine the spontaneous direction and limit of reactions, and it is associated with K_{ads} by following formula [30]:

$$\Delta G^0_{ads} = -RT \ln 1000 K_{ads} \qquad (7)$$

where R is universal gas constant, T represents the absolute temperature. The value of 1000 stands for the concentration of H_2O in the solution (g/L). Generally, a negative ΔG^0_{ads} indicates that the adsorption reaction can be spontaneous.

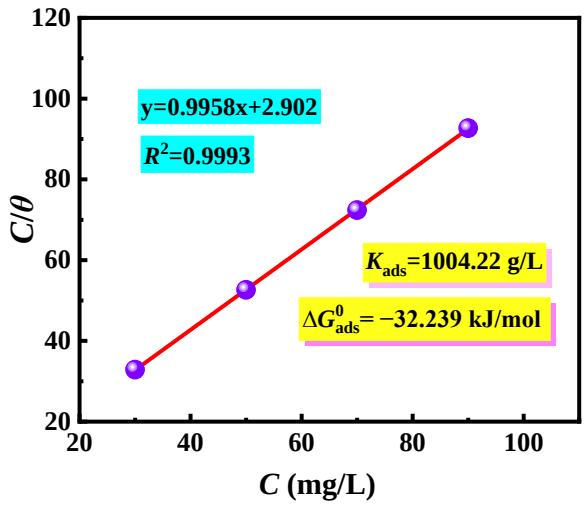

Figure 5. Langmuir adsorption isotherm of MTOI on the N80 surface in HCl medium.

The absolute value of ΔG^0_{ads} less than 20 kJ/mol can be regarded as physisorption, which arising from electrostatic attraction between charged metal surface and corrosion inhibitor. Whereas, the value

greater than 40 kJ/mol is related to chemisorption, which may be caused by charge sharing or transfer between iron atoms and inhibitor molecule [31]. The absolute values of ΔG^0_{ads} calculated in this case is between 20~40 kJ/mol, which suggests that the adsorption of MTOI on the steel surface belongs to the comprehensive effect of physisorption and chemisorption.

3.5. Surface analysis

The morphological features of the surface of N80 steel samples exposed to 15% HCl with and without the presence of optimum concentration of MTOI was examined by SEM and is depicted in Figure 6. Clearly, the polished surface of N80 steel is very smooth, scratches and corrosion are almost non-existent. However, the surface immersed in blank solution is seriously damaged and corroded, and the roughness increment is obvious. In contrast, the surface of the steel in 15% HCl solution with 90 ppm MTOI displays very little roughness and shows relatively smooth surface. According to the EDS analysis, the N, S, and I elements was observed when the steel was treated with MTOI inhibitor, which indicates that the inhibitor molecule can form an acid-resistant barrier film on the steel surface, which slows down the hydrogen evolution reaction and effectively prevents the corrosion of the N80 steel.

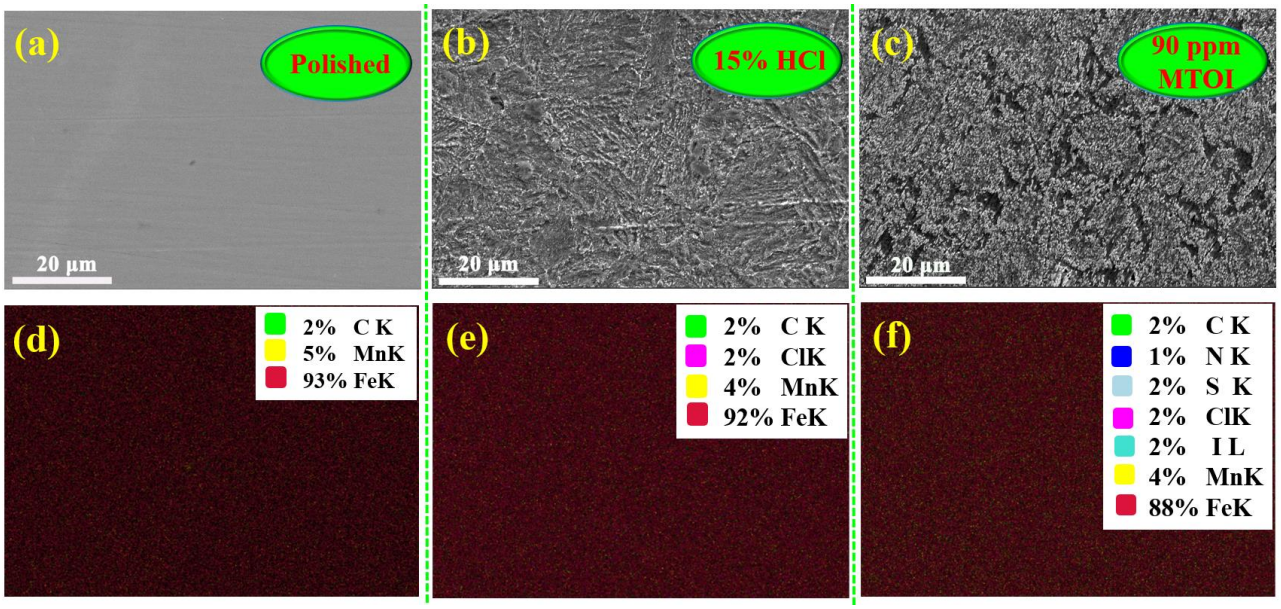

Figure 6. SEM-EDS results of N80 steel under different conditions: (a, d) polished N80 steel, (b, e) immersed in blank solution, (c, f) immersed in 15% HCl solution containing 90 ppm MTOI.

3.6. Theoretical studies

3.6.1. Quantum chemical calculation

In order to determine the preferred adsorption center of MTOI cation and establish the correlation between its molecular structure and inhibition efficiency, DFT based geometric optimization was performed. The frontier molecular orbitals (HOMO & LUMO) distribution and relevant quantum

parameters were presented in Figure 7 and Table 3. Obviously, the HOMO is located over the thiourea moiety while LUMO is concentrated on the double bond of alkyl chain. The electrostatic potential (ESP) provides a distinct electrophilic and nucleophilic attack position. As demonstrated, MTOI exhibits abundant active sites with electrophilic and nucleophilic attacks, and the probability of establishing covalent bonds between electrophilic attack sites and the 3*d* empty orbitals of Fe atoms is relatively high. The electron transfer fraction (ΔN) is an important parameter to provide information about the adsorption capacity of the molecular structural on the metal surface, which can be calculated from the following relationships [32]:

$$\omega = (I + A)/2 = -(E_{HOMO} + E_{LUMO})/2 \quad (8)$$

$$\xi = (I - A)/2 = (E_{LUMO} - E_{HOMO})/2 \quad (9)$$

$$\Delta N = \frac{\omega_{Fe} - \omega_{inh}}{2(\xi_{Fe} + \xi_{inh})} \quad (10)$$

wherein, ω_{Fe} and ω_{inh} signify the absolute electronegativity of iron and the inhibitor molecule, respectively; ξ_{Fe} and ξ_{inh} represent the corresponding hardness. The theoretical values of ω_{Fe} and ξ_{Fe} were set as 7.0 and 0 eV, respectively. Our obtained value of ΔN is positive and less than 3.6, indicating that the trend of the concerned inhibitor to donate its electrons to metal surface is strong, which facilitates the adsorption process by forming a covalent bond [33].

Figure 7. HOMO, LUMO, ESP density distributions for MTOI cation.

Table 3. The quantum chemical variables for MTOI inhibitor based on DFT approach.

E_{HOMO} (eV)	E_{LUMO} (eV)	ΔE (eV)	I (eV)	A (eV)	ω (eV)	ξ (eV)	ΔN
−6.40	−1.35	5.05	6.40	1.35	3.875	2.525	0.618

3.6.2. Molecular dynamic (MD) simulation

The adsorption behavior of MTOI molecule on the Fe (110) surface in aqueous phase was elucidated by MD simulation. When the energy and temperature become balanced, the system reached equilibrium. Figure 8 shows the most stable configuration where the adsorption of MTOI on the Fe (110) surface occurs as top and side views. In order to achieve maximum coverage, the molecules prefer to get adsorbed in parallel mode on the substrate. The density field distribution of MTOI on the metal surface is also given, and it can be hypothesized that the erosion of corrosive particles can be intercepted by the formation of a dense barrier layer in three-dimensional space.

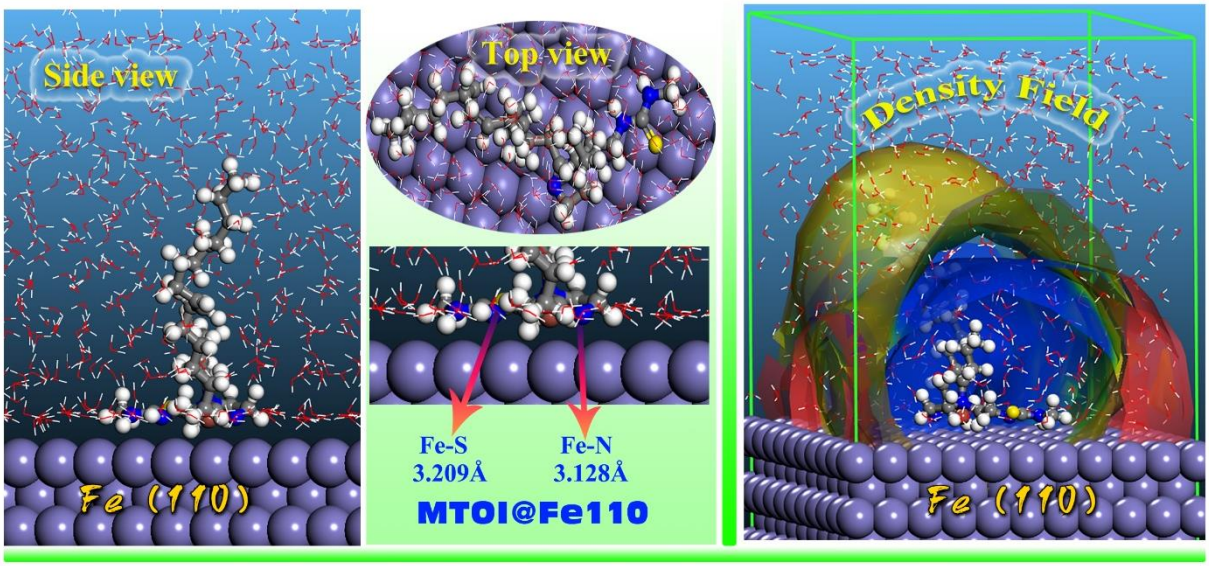

Figure 8. Equilibrium configurations and density field distribution for the MTOI/Fe(110) adsorption system.

To determine the adsorption strength between the inhibitor and metal surface, the chosen descriptor (adsorption energy, E_{ads}) can be estimated by the following formula [34]:

$$E_{ads} = E_{total} - (E_{Fe+solu} + E_{inh+solu}) + E_{solu} \quad (11)$$

where E_{total} is the total energy of whole adsorption system, $E_{Fe+solu}$ stands for the energy of Fe substrate together with solvent molecules, $E_{inh+solu}$ represents the total energy of the inhibitor and solution, E_{solu} denotes the potential energy of the solvent molecules. Generally, a more negative E_{ads} value suggests a stronger adsorption power between the inhibitors and metal surface. The E_{ads} value of the MTOI inhibitor was found to be −557.5 kJ/mol. This negative value indicates that the adsorption system was stable, and that spontaneous adsorption might occur in this scenario. Overall, our theoretical analysis backs up the experimental findings.

3.7. Inhibition and adsorption mechanism

Figure 9 displays the proposed inhibition mechanism of MTOI for N80 steel in HCl solution. Due to the chemical reaction of Fe^{2+} and Cl^- in 15% HCl solution, the dispersed ferric chloride fragments are generated in N80 steel, which weakens the application performance of the metal. When MTOI corrosion inhibitor is added, N and S atoms with lone pair electrons can form chelating agents with empty Fe 3*d* orbitals, which are deposited on the metal surface to form protective film. In addition, the corrosion inhibitor contains long alkyl chains, causing the protective film to have hydrophobicity, effectively preventing the solution to the metal dissolution reaction. More significantly, the MTOI inhibitor contains positively charged cations. It can physically adsorb with Cl^- and I^-, which indirectly retards the anode dissolution reaction [35]. Protonation also decelerates the reduction active site of the cathode by hydrogen ions. These results indicate that the protective film produced by physical & chemical adsorption between MTOI inhibitor and N80 steel positively hinders the corrosion of steel.

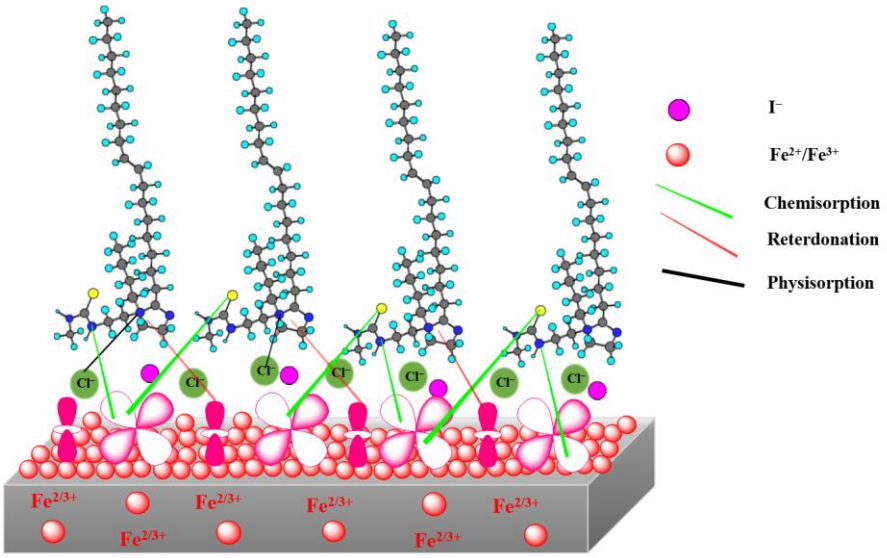

Figure 9. Corrosion inhibition mechanism of MTOI for N80 steel in 15% HCl medium.

4. CONCLUSIONS

In this work, an imidazoline-derived corrosion inhibitor was successfully synthesized, and its corrosion inhibition performance and mechanism for N80 steel in 15% HCl were systematically researched. The main conclusions are as follows:

(1) FTIR identification of some distinct functional groups in the prepared product indicated that MTOI was successfully synthesized.

(2) PDP and EIS data showed that MTOI is a mixed-type corrosion inhibitor. It blocks electron transfer and increases the thickness of the double electric layer, exhibiting obvious corrosion inhibition effect.

(3) The adsorption of MTOI on N80 steel was declared to follow Langmuir adsorption isotherm. The adsorption mode is a combination of physical & chemical adsorption.

(4) Surface analysis confirmed that the heteroatoms N, S as well as anion of MTOI adsorbed on the metal surface to form a compact protective film, which prevented the corrosion of the metal.

(5) The DFT and MD findings confirmed the results obtained from experiments.

ACKNOWLEDGMENTS
Riadh Marzouki extends his appreciation to the Deanship of Scientific Research at King Khalid University for partly funding this work through research groups under grant number R.G.P.2/72/42. This work was sponsored by the National Natural Science Foundation of China (22062022, 52074232), the Science and Technology Program of Guizhou Province (QKHJC[2019]1311), the Foundation of the Department of Education of Guizhou province (QJHKY[2020]067), and the Opening Project of Sichuan University of Science and Engineering, Material Corrosion and Protection Key Laboratory of Sichuan province (2020CL06).

References

1. M. Askari, M. Aliofkhazraei, S. Ghaffari and A. Hajizadeh, *J. Nat. Gas Sci. Eng.*, 58 (2018) 92-114.
2. P. de Lima-Neto, A. P. de Araduo, W. S. Araujo and A. N. Correia, *Prog. Org. Coat.*, 62 (2008) 344-350.
3. C. Verma, E. E. Ebenso, M. A. Quraishi and C. M. Hussain, *Materials Advances*, 2 (2021) 3806-3850.
4. S. Sharma and A. Kumar, *J. Mol. Liq.*, 322 (2021) 114862.
5. L. Guo, R. Zhang, B. Tan, W. Li, H. Liu and S. Wu, *J. Mol. Liq.*, 310 (2020) 113239.
6. L. J. Yu, J. Zhang, G. M. Qiao, Y. G. Yan, Y. Ti and Y. Zhang, *Mater. Corros.*, 64 (2013) 225-230.
7. L. Guo, I. B. Obot, X. Zheng, X. Shen, Y. Qiang, S. Kaya and C. Kaya, *Appl. Surf. Sci.*, 406 (2017) 301-306.
8. A. A. Farag, M. A. Migahed and E. A. Badr, *J. Bio. & Tribo. Corros.*, 5 (2019) 53.
9. P. Kannan, A. Varghese, K. Palanisamy and A. S. Abousalem, *J. Mol. Liq.*, 297 (2020) 111855.
10. T. E. Schmitzhaus, M. R. Ortega Vega, R. Schroeder, I. L. Muller, S. Mattedi and C. d. F. Malfatti, *Mater. Corros.*, 71 (2020) 1885-1902.
11. A. Klamt, C. Moya and J. Palomar, *J. Chem. Theory Comput.*, 11 (2015) 4220-4225.
12. M. Meunier and S. Robertson, *Mol. Simul.*, 47 (2021) 537-539.
13. H. Sun, P. Ren and J. R. Fried, *Comput. Theor. Polym. Sci.*, 8 (1998) 229-246.
14. L. Guo, B. Tan, W. Li, Q. Li, X. Zheng and I. B. Obot, *J. Mol. Liq.*, 327 (2021) 114828.
15. M. Boulhaoua, M. El Hafi, S. Zehra, L. Eddaif, A. A. Alrashdi, S. Lahmidi, L. Guo, J. T. Mague and H. Lgaz, *Colloids Surf. A*, 617 (2021) 126373.
16. O. Dagdag, A. El Harfi, O. Cherkaoui, Z. Safi, N. Wazzan, L. Guo, E. D. Akpan, C. Verma, E. E. Ebenso and R. T. T. Jalgham, *RSC Adv.*, 9 (2019) 4454-4462.
17. L. El Hamdaoui, M. El Marouani, M. El Bouchti, F. Kifani-Sahban and M. El Moussaouiti, *ChemistrySelect*, 6 (2021) 306-317.
18. R. Westphal, J. W. de Souza Pina, J. P. Franco, J. Ribeiro, M. Delarmelina, R. G. Fiorot, J. W. de Mesquita Carneiro and S. J. Greco, *Adv. Chem. Eng. Sci.*, 10 (2020) 378-398.
19. A. Zomorodian, R. Bagonyi and A. Al-Tabbaa, *J. Build. Eng.*, 38 (2021) 102171.
20. W. Emori, V. M. Bassey, H. Louis, P. C. Okonkwo, S. Zhao, K. Wei, P. C. Okafor, J. Wan and C.-R. Cheng, *Bioelectrochemistry*, 141 (2021) 107840.
21. D. Kesavan, M. Gopiraman and N. Sulochana, *Chem. Sci. Rev. Lett.*, 1 (2012) 1-8.
22. X. Zheng, M. Gong, Q. Li and L. Guo, *Sci. Rep.*, 8 (2018) 9140.
23. W. Zhang, H. J. Li, L. Chen, S. Zhang, Y. Ma, C. Ye, Y. Zhou, B. Pang and Y. C. Wu, *Carbohydr. Polym.*, 238 (2020) 116216.
24. W. W. Li, Z. Zhang, Y. Zhai, L. Ruan, W. P. Zhang and L. Wu, *Int. J. Electrochem. Sci.*, 15 (2020) 722-739.
25. G. J. Brug, A. L. G. Vandeneeden, M. Sluytersrehbach and J. H. Sluyters, *J. Electroanal. Chem.*, 176 (1984) 275-295.
26. J. Haque, V. Srivastava, D. S. Chauhan, H. Lgaz and M. A. Quraishi, *ACS Omega*, 3 (2018) 5654-5668.
27. J. H. Tan, L. Guo, D. Wu, X. J. Duan, S. L. Leng, I. B. Obot and S. Kaya, *Int. J. Electrochem. Sci.*, 15 (2020) 8837-8848.
28. B. E. Conway, J. O. M. Bockris and I. A. Ammar, *Trans. Faraday Soc.*, 47 (1951) 756-766.
29. A. Mittal, L. Kurup and J. Mittal, *J. Hazard. Mater.*, 146 (2007) 243-248.
30. M. S. Walczak, P. Morales-Gil and R. Lindsay, *Corros. Sci.*, 155 (2019) 182-185.
31. S. Aourabi, M. Driouch, M. Sfaira, F. Mahjoubi, B. Hammouti, C. Verma, E. E. Ebenso and L. Guo, *J. Mol. Liq.*, 323 (2021) 114950.
32. I. B. Obot, D. D. Macdonald and Z. M. Gasem, *Corros. Sci.*, 99 (2015) 1-30.

33. M. Zhang, L. Guo, M. Zhu, K. Wang, R. Zhang, Z. He, Y. Lin, S. Leng, V. Chikaodili Anadebe and X. Zheng, *J. Ind. Eng. Chem.*, 101 (2021) 227-236.
34. R. Hsissou, S. Abbout, Z. Safi, F. Benhiba, N. Wazzan, L. Guo, K. Nouneh, S. Briche, H. Erramli, M. Ebn Touhami, M. Assouag and A. Elharfi, *Constr. Build. Mater.*, 270 (2021) 121454.
35. J. Tan, L. Guo, D. Wu, R. Yu, F. Zhang and S. J. I. J. E. S. Kaya, *Int. J. Electrochem. Sci.*, 15 (2020) 1893-1903